Influence of the thermal boundary conditions on the heat transfer of a rib-roughened cooling channel using LES

S. Scholl - T. Verstraete* - J. Torres-Garcia† - F. Duchaine‡ - L. Y. M. Gicquel‡*

*Turbomachinery and Propulsion Department, von Karman Institute for Fluid Dynamics,
Chaussee de Waterloo 72, Rhode-St.-Genese, Belgium.
corresponding E-Mail: sebastian.scholl@vki.ac.be

† Polytechnic University of Valencia, s/n 46022 Valencia, Spain.

‡ CERFACS, 42 Avenue Gaspard Coriolis, 31057 Toulouse Cedex 01, France.

ABSTRACT

Internal cooling channels of turbine blades are rib-roughened to increase the heat transfer between the wall and the coolant. A large effort has been made in simulating these flows with Large Eddy Simulations (LES) to have a better understanding of the flow physics. This contribution focuses on the thermal prediction capabilities of LES for such cooling channels. Of particular interest to this study is the influence of the thermal boundary condition on the heat transfer coefficient. If important, this strongly indicates that conjugate effects exist that would need to be modeled resulting in significant additional computational cost. Studies were carried out for Reynolds numbers of 40,000 at different thermal uniform heat flux boundary conditions. The results are compared with experimental aerodynamic and thermal data obtained at the Von Karman Institute for Fluid Dynamics. The main outcomes are: First, the results show the dependence of the heat transfer coefficient on the imposed thermal boundary condition, even though it is usually assumed in experimental and numerical studies to depend only on the aerodynamics; this assumption may not be valid. Second, the dependence of the heat transfer coefficient on the thermal boundary condition implies that conjugate heat transfer is important for the current configuration and can be captured numerically, although research on fully coupled, efficient LES based conjugate heat transfer algorithms is still needed.

NOMENCLATURE

c	speed of sound	$[ms^{-1}]$
D_h	Hydraulic diameter	$[m]$
EF	enhancement factor	
F	flux tensor	
f	friction factor	
H	rib height	$[m]$
h	heat transfer coefficient	$[Wm^{-2}K]$
L	length of channel model	$[m]$
Ma	Mach number	
Nu	Nusselt number	
P	pitch length in the ribbed channel	$[m]$
p	pressure	$[Nm^{-2}]$
Pr	Prandtl number	
q	heat flux	$[Wm^{-2}]$
r	gas constant	$[J^1K^{-1}mol^{-1}]$
Re	Reynolds number	

T	temperature	$[K]$
TR	temperature ratio	
t	time	$[s]$
u, v, w	velocity components	$[ms^{-1}]$
W	vector of primary variables	
w	quantity at the wall	
$y+, x+, z+$	non-dimensional measures of the first cell to the wall	
Δx	grid cell size	$[m]$
Δt	time step	$[s]$
ν	kinematic viscosity	$[m^2 s^{-1}]$
μ	dynamic viscosity	$[Pa^1 s^1]$
ρ	density	$[kg^1 m^{-3}]$
λ	thermal fluid conductivity	$[Wm^{-1}K^{-1}]$
τ_w	wall shear stress	$[Wm^{-1}K^{-1}]$
CFL	Courant-Friedrich-Levy number	
LES	Large Eddy Simulation	
NSCBC	Navier-Stokes Characteristic Boundary Condition	
PIV	Particle Image Velocimetry	
SGS	Sub-grid Scale	
RANS	Reynolds-averaged Navier-Stokes	
∞	free stream quantity	

INTRODUCTION

Trying to comply with the claims for environmental awareness and the rising use of energy, the turbomachinery industry improves the gas turbine efficiency by several means, one of which consists in increasing the turbine inlet temperature to increase the turbine cycle efficiency. In modern gas turbine engines, the turbine inlet temperature exceeds the metal melting temperature such that internal and external cooling techniques need to be applied and developed. Since the life of a turbine blade is reduced by half with an increased turbine solid temperature of only 30 Kelvin (Han 2000), the prediction of local heat transfer coefficients and temperatures is a crucial step towards the design of high pressure turbine blades and vanes. Current numerical methods lack the needed capacity to accurately predict the wall temperature and call for new numerical strategies. Reynolds-averaged Navier-Stokes simulations, for instance, fail to predict complex flow fields and can lead to wrong thermal predictions. For the present investigation of an internal, rib-roughened cooling channel, Large Eddy Simulations (LES) have been used, which improve the turbulent flow field and heat transfer predictions.
The heat transfer coefficient is a frequently used engineering parameter during the thermal design. It is derived from Newton's law of convection:

$$q = h(T_w - T_\infty), \tag{1}$$

with the wall temperature T_w, the free-stream temperature T_∞, the heat flux q and the heat transfer coefficient h. In practice, the heat transfer coefficient is used to impose convective boundary conditions at the solid walls to obtain a temperature field inside the blade. For these calculations, it is normally assumed that the heat transfer coefficient is only dependent on the aerodynamics (Maffuli and He 2013), such that external influences to the flow imposed through thermal boundary conditions (whether as iso-thermal, iso-flux or non-uniform thermal boundary conditions) and the inlet to wall temperature ratio would not affect the heat transfer coefficient. However, few studies do indicate that the heat transfer coefficient is not independent of the temperatures. Fitt et al. (1986) showed an influence of the temperature on the heat transfer coefficient analytically for a laminar boundary layer. More recently, Maffuli and He (2013) observed a non-linear dependence of the heat transfer coefficient on the temperature ratio, between fluid inlet and wall, on a 2D Nozzle Guide Vane using RANS simulations.

Of particular interest to this study is the influence of the thermal boundary condition on the heat transfer coefficient, questioning the assumption of a constant heat transfer coefficient for a turbulated cooling channel. A non-constant heat transfer coefficient indicates that thermal influences external to the fluid have an impact on the solution within the fluid domain and should be included when solving the thermal problem. Therefore, a conjugate heat transfer problem needs to be solved in which not only the aerodynamics, but also the heat transfer in the solid are included and solved in a coupled manner. A coupled approach, especially based on LES, would lead to significant additional computational costs due to the differences in the time scales for the fluid and solid domain, both differing by orders of magnitude. Currently with Large Eddy Simulations, research is still needed for an efficient LES based CHT Strategy (e.g., Duchaine et al. 2009), which would be needed to be addressed in further studies. Experimental studies did recently indicate a conjugate effect (Cukurel and Arts (2013)). An objective of this study is whether this experimental observation can be found to be true numerically via LES, while bypassing real conjugate computations by applying different flux boundary conditions and thus reducing the computational cost.

NUMERICAL METHOD

The fluid flow was computed by the CERFACS in-house LES solver AVBP (Schönfeld and Poinsot, 1999; Mendez and Nicoud, 2008). Applying Favre filtering to the unsteady, compressible Navier-Stokes equations (Sagaut 2000), leads to the following LES equations:

$$\frac{\partial \bar{W}}{\partial t} + \nabla \cdot \bar{F} = 0, \tag{2}$$

with the conservative variables $\bar{W} = (\bar{\rho}, \bar{\rho}\tilde{u}, \bar{\rho}\tilde{v}, \bar{\rho}\tilde{w}, \bar{\rho}\tilde{E})$ the flux tensor $\bar{F}$, the density $\bar{\rho}$, the velocity components $(\tilde{u}, \tilde{v}, \tilde{w})$, and the total Energy $\tilde{E}$. The fluid follows the Favre filtered equation of state $\bar{p} = \bar{\rho} r \tilde{T}$, with the gas constant r. The conductive heat flux is included in the flux tensor and given by Fourier's law of conduction:

$$\bar{q_i} = -\bar{\lambda}\frac{\partial \tilde{T}}{\partial x_i}, \tag{3}$$

with the thermal conductivity

$$\bar{\lambda} = \frac{\bar{\mu}(\bar{T}) c_p(\bar{T})}{Pr}, \tag{4}$$

where c_p is the specific heat at constant pressure, Pr the Prandtl number and $\bar{\mu}$ the dynamic viscosity. The solver uses tabulated values for the temperature dependent specific heat at constant pressure. The fluid viscosity follows a temperature dependent power law. The unknowns appearing in the LES equations, i.e. the subgrid-scale (SGS) quantities, need to be modeled. The Boussinesq eddy viscosity assumption is applied for which a subgrid-scale turbulent viscosity ν_t is modeled via the Wall Adapting Linear Eddy (WALE) model (Nicoud and Ducros 1999). Using the SGS turbulent viscosity, the SGS turbulent conductivity is modeled as $\lambda_t = \bar{\rho}\nu_t c_p / Pr_t$, with the turbulent Prandtl number fixed at $Pr_t = 0.7$. The equations are discretized by centered spatial schemes and explicit time schemes with a Finite-Element based two step Taylor-Galerkin (TTGC) scheme for the convection in a cell-vertex formulation (Colin and Rudgyard, 2000 and Donea and Huerta 2003). This explicit scheme is of third order accuracy in space (on hybrid meshes) and time, providing low dissipation, especially suitable for LES. The diffusion term is discretized with a vertex-centered operator closely following the Galerkin method and is of second order, having a $\Delta 2$ stencil (Colin et al., 2003 and Donea and Huerta 2003). The time step is controlled via the Courant-Friedrich-Lewy (CFL) condition for compressible

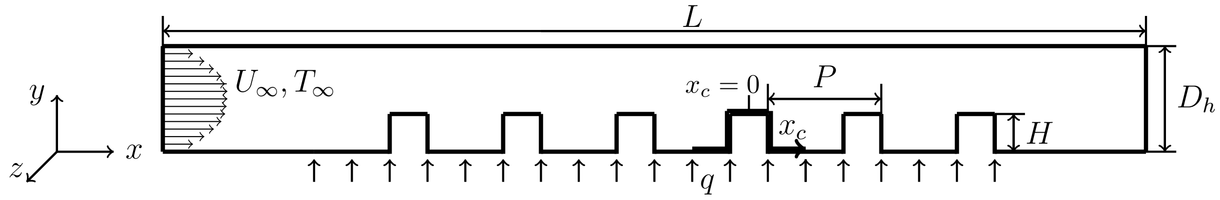

Figure 1: Sketch of the channel geometry.

flows: $CFL = \frac{(U+c)\Delta t}{\Delta x} \simeq 0.7$, with the smallest grid cell size Δx and the minimal Δt in the whole domain, U and c being the local flow and sound speeds. The Navier-Stokes Characteristic Boundary Conditions (NSCBC) of Poinsot and Lele (1992), are applied at the inlet and the outlet.

TEST CASE AND COMPUTATIONAL SETUP

Configuration

Parameter	abbr.	Value
Reynolds number	Re_{D_h}	40,000
number of ribs		6
length	L	1597.5 mm
hydraulic diameter	D_h	75 mm
rib height	H	22.5 mm
pitch to rib ratio	P/H	10
blockage ratio	H/D_h	0.3

Table 1: Channel and flow characteristics (Cukurel 2012).

The applied configuration models the experimental facility of Çakan (2000), Cukurel (2012) and Cukurel and Arts (2013), which was a simplified model of an internal rib-roughened aircraft gas turbine blade cooling passage with a pitch to rib ratio of 10 and a blockage ratio of 0.3 (Table 1 summarizes dimensions). The cooling passage was scaled up by a factor of 15 with respect to real engine conditions (Cukurel, 2012). The scaling ratios for the experiments resulted from a compromise between the need for high measurement resolution and limiting electrical power supply (Çakan 2000). The experimental facility consisted of three sections: an inlet, a test and an outlet section from which the test section with its six ribs was fully represented by the configuration for the numerical simulations (Fig. 1). Only a part of the inlet and outlet sections were simulated with appropriate boundary conditions. The cross section dimensions were 75x75 mm and the test section length was 1260 mm. Although the rib of the cooling channel repeats itself periodically, the total number of six ribs was kept similar to the experimental model to avoid possible arbitrary effects of periodic boundary conditions that occur as Fransen et al. (2012) have shown.

Flow and boundary conditions

No-slip conditions were applied at all walls. The inlet and outlet boundaries are positioned far from the actual part of interest avoiding major influences on the flow around the ribs. Adiabatic conditions were applied on the lateral walls and the top wall, while iso-flux boundary conditions were applied to the rib-surrounding surface. Keylock et al. (2011) demonstrated on a single rib with a lower blockage ratio (0.15) than in the present study that the rib has such a strong effect on the flow that the precise nature of the inlet condition, with regards to the turbulent fluctuations and length scales, is forgotten and only small differences for the flow separation and reattachment may appear. The reattachment lengths and many flow quantities will be preserved reasonably well, regardless of the inlet profile. Due to the even larger blockage ratio used in this study, a turbulent mean profile without fluctuations for the flow was applied as inlet condition. At the outlet, the static pressure was set. To simulate the exact flow conditions with the small Mach number of the experimental campaign of Cukurel (2012) at Ma = 0.02, the computational time (using a compressible solver with explicit time integration) would have been unjustifiably long. Hence, the Mach number was increased to Ma = 0.2, keeping the same Reynolds number, based on the bulk velocity and the hydraulic diameter, at 40,000. This scaling granted a decrease of the computational cost and a re-scaling to more real engine conditions, while maintaining the similarity with the experimental data and keeping the simulated Mach number small enough to avoid compressibility effects.

Mesh description

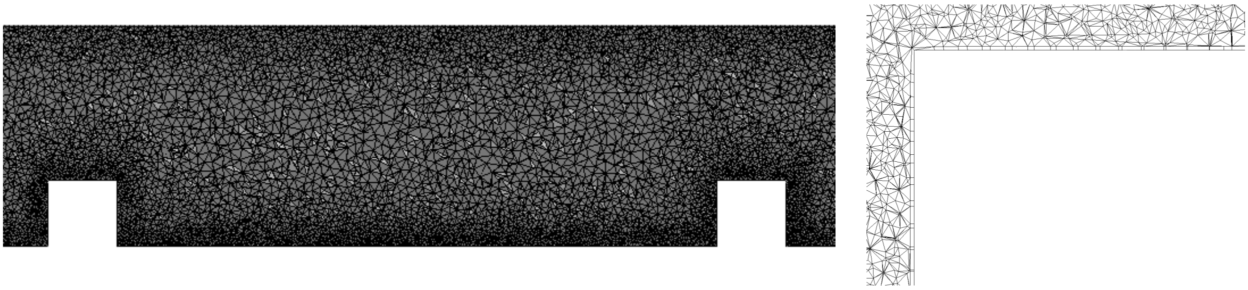

(a) Mesh around two ribs (b) mesh around rib corner

Figure 2: Mesh around two ribs and rib corner.

Due to the ubiquitous presence of walls in the internal cooling passage and the need for resolving the walls instead of using wall-functions to obtain a realistic heat transfer coefficient, the mesh requirements are high, leading to demanding and costly wall-resolved LES.
The unstructured LES solver AVBP was in particular designed to deal with hybrid meshes, therefore a hybrid mesh (consisting of tetrahedra within the channel and prisms at the walls) has also been used for the current application. Figure 2(a) shows the tetrahedra of a used mesh around two ribs of the channel in the symmetry plane. To obtain the correct temperature and heat transfer, the closest grid point needs to be within the viscous sublayer, leading to small grid cells at the wall. A prismatic layer in the wall-normal direction provides a good orthogonality and needs less elements for the same resolution than a tetrahedral layer. Finally, prismatic layers reduce (with a larger possible aspect ratio and cell volume) the constraints on the time steps that are required for stability. Figure 2(b) shows a zoom at the corner of a rib visualizing the prism layer. Fransen et al. (2012) and Fransen (2013) observed that using one prism layer results in the best mesh quality for a hybrid mesh in such a ribbed geometry. Increasing the amount of prism layers penalized the quality in the rib to bottom wall corners.

RESULTS AND DISCUSSION

The following section first presents a mesh convergence study showing five levels of refinement. After assessing the quality of the used mesh and the aerodynamics field, the section shows the results for the heat transfer comparing two different cases. Both cases were done with the highest quality mesh, resulting from the mesh study, at 12,000W/m^2 and 120,000W/m^2 comparing each others heat transfer enhancement to observe the dependency of the heat transfer coefficient on the boundary condition.

Enhancement Factor and mesh convergence

A comparison of different mesh resolutions resulting in a convergence study, and its effect on the enhancement factor (EF) has been done. The enhancement factor quantifies the increase of heat transfer in comparison with a correlation valid for flow in a smooth pipe at the same Reynolds number. It is defined as:

$$EF = \frac{Nu}{Nu_0}. \tag{5}$$

The Nusselt number is defined as:

$$Nu = \frac{h \cdot D_h}{\lambda(T)}, \tag{6}$$

with the heat transfer coefficient h, the hydraulic diameter D_h and the fluid conductivity λ . The Dittus-Boelter correlation (Dittus and Boelter 1930) gives the denominator for the enhancement factor (valid for $0.7 < Pr < 120$) and is defined as: $Nu_0 = 0.023 Re_{D_h}^{4/5} Pr^{0.4}$. The heat transfer coefficient h is defined as in Eq. (1), while T_∞ is defined as the bulk temperature T_{bulk}. Due to uniform heating and periodical flow conditions, the bulk temperature is assumed to linearly increase inside the channel. Considering the values around ribs, the linear increase of the bulk temperature is further simplified with a sequence of step functions (which results in a constant bulk temperature along the pitch). This assumption allowed a fair comparison with previous results, which used the same data reduction approach (Çakan, 2000). A mass flow average was used for the inlet and outlet temperatures of the simulations.

Table 2 summarizes the mesh properties. Mesh M1 lacked quality to resolve major flow structures. From mesh M2 on, using a higher resolution and a prism layer in the boundary layer, the aerodynamics were well represented, but till mesh M3 the heat transfer kept increasing (Fig. 3(a)). Mesh M4 had a higher resolution mainly in the channel mid-section. To further improve the heat transfer predictions, mesh M5 used larger cell aspect ratios of wall prisms, while still remaining lower than 8 ($\Delta z \simeq \Delta x \simeq AR \cdot \Delta y$), as Sagaut (2000) suggests. The histograms in Fig. 3(b) and Fig. 3(c) present the y+ distribution around the ribs for the meshes M4 and M5. The smaller wall distance of the first grid point of mesh M5 (and the larger aspect ratios of M5 to keep a reasonable cell count) lead to a beneficial y+ distribution in comparison with M4, keeping the majority of first node distances within the viscous sub-layer and $y+ < 5$. Collado Morata et al. (2012) have recently shown (on a turbine blade) that with the used solver and numerical schemes a y+ value of 4 leads to good predictions for the heat transfer. The mean y+ value for meshes M3 and M4 are around this value while the value for mesh M5 is even smaller. Since the heat transfer changed very little (Fig. 3(a)) from mesh M4 to mesh M5, the result for mesh M5 can be considered grid-converged. Hence, mesh M5 is assumed to deliver reliable results and will be used for the analyses in the following sections.

	mesh M1	mesh M2	mesh M3	mesh M4	mesh M5
cells	3.53M	8M	10.5M	20.6M	20.3M
nodes	0.69M	1.5M	2M	3.86M	3.74M
prisms	no	yes	yes	yes	yes
mean y+	18.72	8	4.1	4.1	3.4
x+,z+	~ 1	~ 5	~ 5	~ 5	~ 8

Table 2: Used meshes. y+ is defined using the wall-normal distance y, the friction velocity u_τ the wall shear stress τ_w as: $y+ = \frac{u_\tau y}{\nu}$. x+ and z+ are defined with the streamwise and spanwise mesh resolution, determining the aspect ratio of the cell.

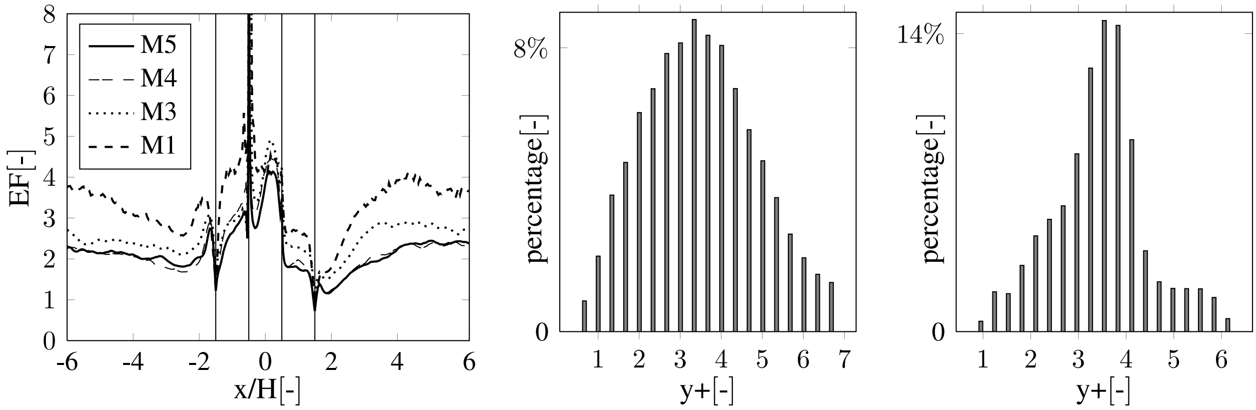

(a) EF around rib n^0 4. View on the bottom surface with the front and back surfaces of the rib unfolded.

(b) $y+$ distribution for mesh M4.

(c) $y+$ distribution for mesh M5.

Figure 3: EF of used meshes along the unfolded rib and y+ value distribution around the ribs of the meshes. y+ is defined using the wall-normal distance y, the friction velocity u_τ the the wall shear stress τ_w as: $y+ = \frac{u_\tau y}{\nu}$.

Aerodynamic analysis

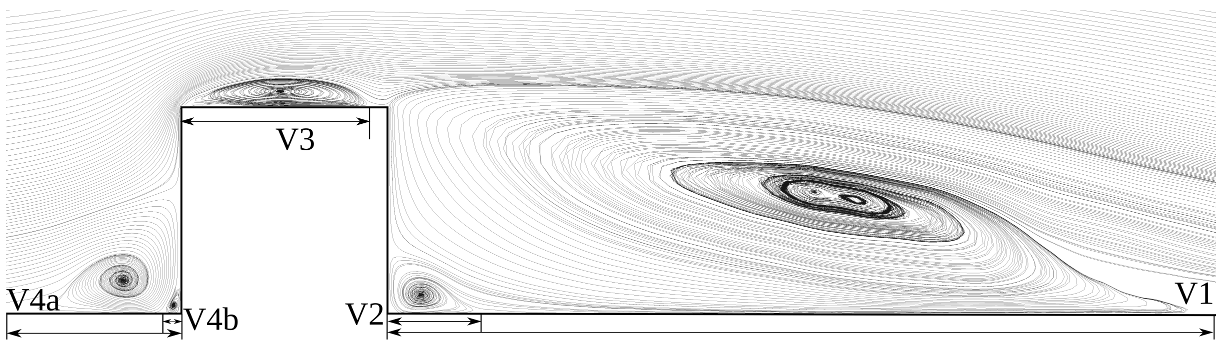

Figure 4: Recirculating zones at rib n^0 4 visualized with streamlines in the center plane.

The following section presents results for time-averaged statistics. The averaging time of the simulations was equivalent to 22 flow throughs, which is the time a fluid particle needs to travel through the whole channel, based on the bulk velocity. Note that the channel contains six ribs, which would translate to 132 flow throughs in a periodic case, ensuring sufficient statistical convergence.
The streamlines in Fig. 4 show the four main recirculation zones in streamwise direction. Table 3 compares their lengths with the experimental study of Casarsa (2003) as well as Casarsa and Arts (2005). The values of the recirculation lengths are evaluated by applying the criteria defined by Casarsa (2003) to assure a direct comparison. The reattachment lengths are therefore measured at a

	V1	V2	V3	V4a	V4b
exp. (Casarsa, 2003)	3.76H-3.84H	0.225H-0.28H	0.6H-0.9H	1.04H-1.5H	-
simulation, case 1	3.7H	0.31H	0.86H	1.46H	0.07H
simulation, case 2	4.09H	0.36H	0.84H	1.69H	0.03H

Table 3: Sizes of recirculation zones in the symmetry plane in streamwise direction (see Fig. 4).

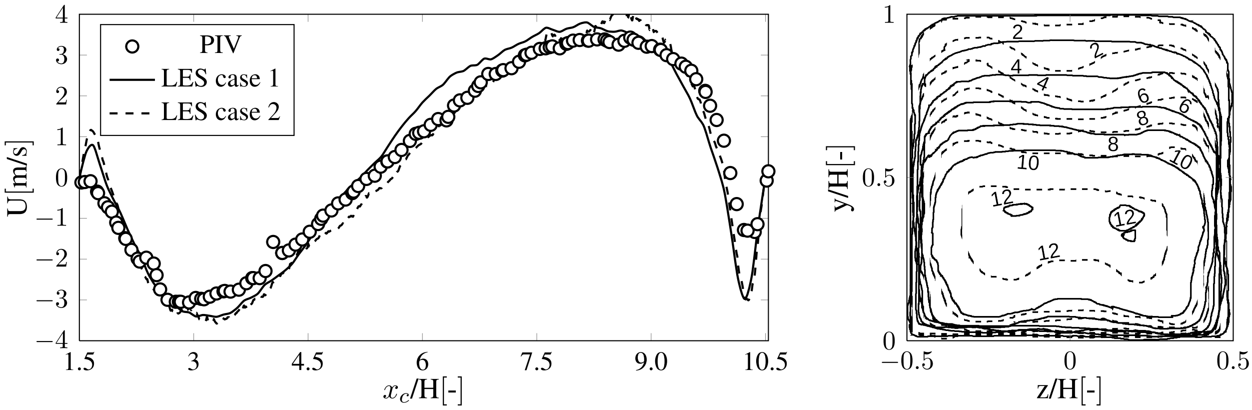

(a) Streamwise velocity at $y/H = 0.05$. (b) Isotachs, u[m/s] at $x_c = 6$

Figure 5: Streamwise velocity comparisons: (a) between experimental and numerical data along the symmetry plane at $y/H = 0.05$; (b) between the two LES cases. Results for experiments by Casarsa (2003). Note: value for LES results have been divided by the scaling factor for comparison.

small distance above the wall with a negative streamwise velocity for V1 at $y/H = 0.05$ and for V3 at $y/H = 0.01$, a positive streamwise velocity for V2 at $y/H = 0.05$ and a vertical velocity, exceeding a threshold of 0.05m/s (scaled for LES) at $y/H = 0.05$.
Comparing the first LES case with 12,000W/m^2 iso-flux boundary condition, the separation downstream of the rib (V1) is in good agreement with the measurement, being close to the range of the experimental uncertainty. The downstream corner region (V2) is only slightly overestimated. The recirculation bubble sizes agree well for the top (V3) and front (V4a) regions. We also found a small recirculation region in the upstream corner (V4b) (using a measurement criterion of $y/H = 0.005$) that has not been observed prior to this study, to our knowledge.
Figure 5 (a) shows the streamwise velocity in the symmetry plane at $y/H = 0.05$, comparing the present LES with the experiment of Casarsa and Arts (2005) showing good agreement. More detailed quantitative results with respect to the aerodynamics were compared with the experimental data (isothermal) of Casarsa (2003), and Casarsa (2005), which are in good agreement as Fig. 6 shows. The secondary flow structures as shown by time averaged spanwise and vertical velocity components are qualitatively and quantitatively well represented by the simulations.
The average pressure drop over one pitch interval is also an important integral parameter to demonstrate the simulation quality (Arts et al. 2007). The pressure drop is expressed using the friction factor:

$$f = \frac{D_h \Delta P}{2L\rho U^2}, \tag{7}$$

with L being the pitch lengths. The rib effect can be demonstrated by normalizing the friction factor with the friction factor for a smooth pipe $f_0 = 0.046Re^{-0.2}$. Table 4 shows the ratio of these friction factors for the simulation compared with an experiment. The difference between the experiment and the simulation is less than 6% which validates the simulations.

	f/f_0
experiment (Casarsa, 2003)	12.3 $\pm$ 0.25
simulation	13.3

Table 4: Normalized friction factor.

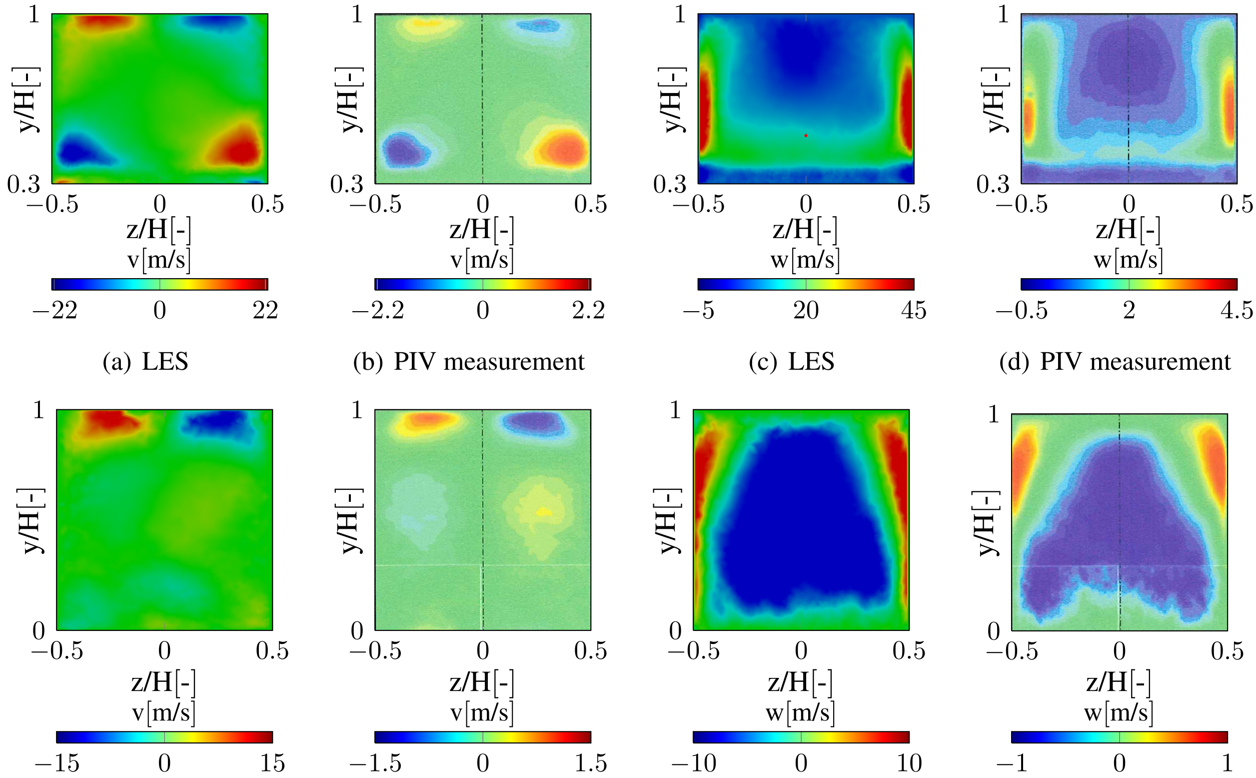

(a) LES (b) PIV measurement (c) LES (d) PIV measurement

(e) LES (f) PIV measurement (g) LES (h) PIV measurement

Figure 6: Time averaged spanwise (a, b, e, f) and vertical (c, d, g, h) velocity component contour plots on the rib (a-d, streamwise coordinate $x_c/H = 0$, see Fig. 1.) and on the pitch (e-h, streamwise coordinate $x_c/H = 5.16$) of the channel.

Heat transfer analysis

For the convective computations, iso-flux boundary conditions were applied around the ribs. The imposed iso-flux boundary condition for the experiment of Cukurel (2012) was 1200W/m^2K. Since we scaled the channel as explained in the previous chapter by a factor of 10 and since we want to keep the Nusselt number constant with the same conductivity in the fluid, the characteristic length is now 10 times smaller, such that the heat transfer coefficient will be 10 times larger. To keep the same temperature ratio from inlet to the wall, the flux needs to be increased by a factor of 10 to keep dimensionally similar conditions.

Figure 7 shows the heat transfer on the bottom surface in terms of the enhancement factor around rib n^0 4 of the channel and shows a good agreement with the experimental results of Cukurel 2012. The overall level of the EF in the experiments and simulation is in very good agreement. Moreover, the effect of the secondary vortical structures on the EF is well visible in the EF contour plot. Only at the front and top parts of the rib the EF level differs quantitatively. A reason for parts of this discrepancy could be lateral conduction in the experiment, since it is very difficult to impose iso-flux boundary conditions on the edges without any lateral conduction, thus smoothing temperature peaks that occur in the numerical simulations.

The relative bulk flow temperature (or temperature ratio) $\frac{T_\infty}{\Delta T}$ was assumed to have only a small effect on the heat transfer in the experiments (Cukurel and Arts 2013), and it is assumed that the Nusselt number depends only on the Reynolds number, the conductivity ratio between fluid and solid and the Biot number: $Nu = f(Re, K, Bi)$. To investigate the validity of this assumption, a second computation with a iso-flux boundary condition, increased by one order of magnitude in comparison with the first simulation, was done. In contrast to the assumption that the temperature ratio is negligible,

	Rib						
	Upstream	Top	Downstream	Mean	Inter Rib	Average	Increase
experiment*	3.2	2.86	1.89	2.65	2.2	2.31	-
LES 12,000W/m^2	2.65	3.72	1.7	2.7	2.04	2.2	-
LES 120,000W/m^2	3.8	3.68	1.89	3.12	2.35	2.48	13%

Table 5: Enhancement Factor comparison; *experiment by Cukurel and Arts (2013).

Fig. 8 shows that there is indeed an influence of the inlet to wall temperature ratio on the heat transfer coefficient or respectively the enhancement factor. Globally, the enhancement factor varies by 13 % (Table 5 summarizes all values for the enhancement factor). The largest difference between both simulations appears at the rib front (Fig. 8 (b)), where the difference is on average 43 % and locally more than 100%.
The changes of fluid properties (viscosity and density) in the channel, especially close to the walls exposed to the iso-flux boundary conditions lead to changes in the aerodynamics, as Table 3 shows,

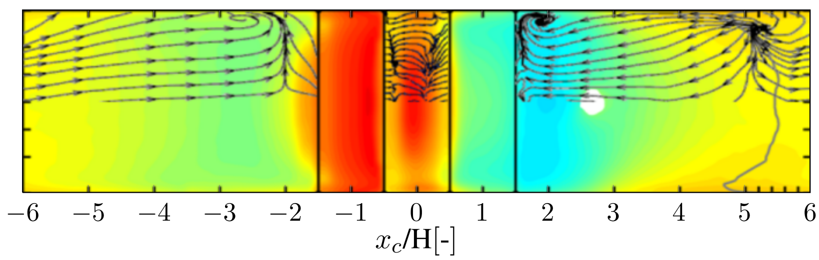

(a) Experiment (Cukurel 2013) with flux kept constant.

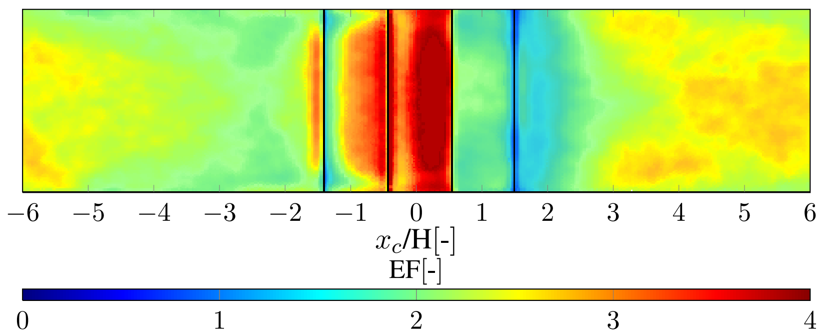

(b) LES with iso-flux boundary conditions.

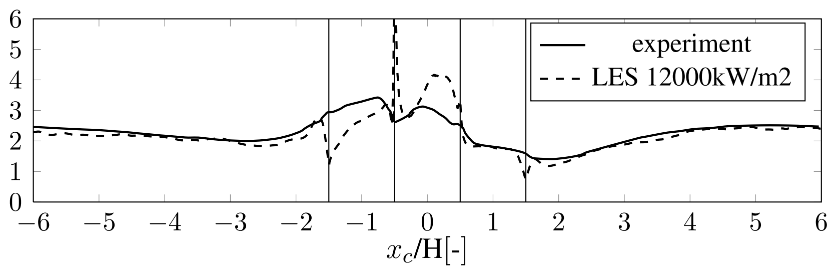

(c) EF for LES and experiment around unfolded rib.

Figure 7: EF contour plot over rib n^0 4 for convective computations (b) in comparison with experiment (a). View on the bottom surface with the front and back surfaces of the rib unfolded. Quantitative comparison between LES and experiment EF (c).

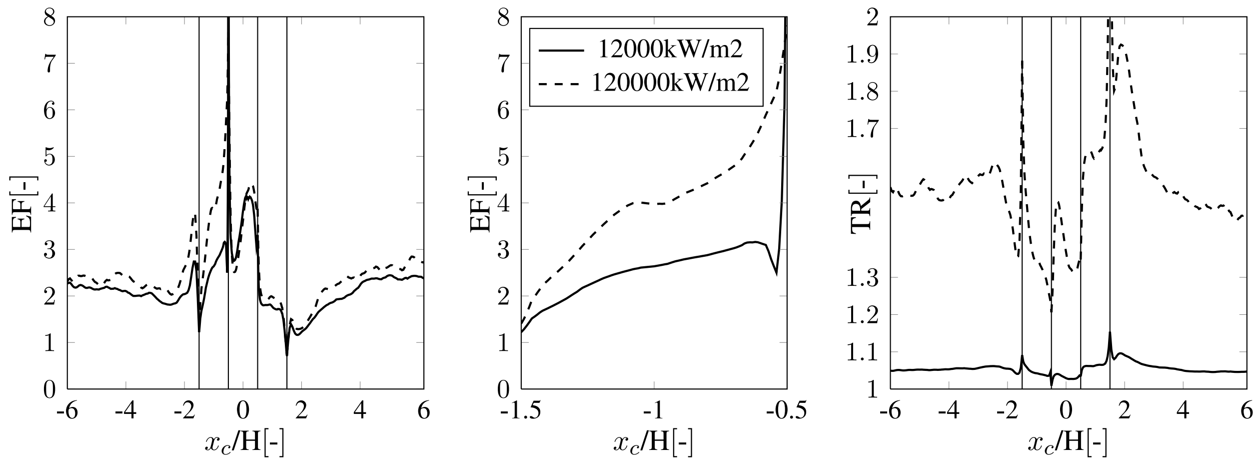

(a) EF around rib $n4$ (b) EF at rib front (c) Temperature ratio (T/T_∞) around rib

Figure 8: EF over rib n^0 4 (a) and the rib front (b) and the temperature around the rib for two different convective computations.

where the recirculation zones of different vortices are compared between the two cases. The larger recirculation zone V1 leads to an accelerated flow downstream, stronger impacting the next rib (Fig. 5 (a) and (b)), leading to a modified heat transfer. In addition, due to changes of the fluid temperature, the fluid conductivity $\lambda(T)$ changes and thus also alters the heat transfer (Fig. 9(a)).

In discussing the differences between both computations, a review of the definition of the heat transfer coefficient (Eqn. 1) with the bulk temperature T_{bulk} is inevitable. The choice of a linearly increasing bulk temperature along the channel introduces errors as Fig. 9 (b) shows, where T_{bulk} is compared with the time-averaged temperature along the centerline for both cases. Moreover, the flow conditions in the channel are far from the assumptions of an ideal thermal boundary layer, as it is found on a heated flat plate, for which Eqn. 1 is more suited. It assumes the temperature reaches a constant value outside of the thermal boundary layer, which is not present in the current investigation as Fig. 9 (c) demonstrates. It shows non-dimensionalized temperatures for both cases starting perpendicular from the rib front at different heights, until reaching upstream the previous rib. Regarding the rectangular geometry of the heated walls, it is apparent that an unambiguous choice for the bulk temperature cannot be made. Also, none of the temperature distribution reaches unity, meaning the bulk flow temperature. Nevertheless, the change in channel aerodynamics, the choice and approximations of the reference output quantities of interest and the change in density, viscosity and fluid conductivity cannot solely explain the large differences for the heat transfer coefficient with the changed thermal boundary condition. It is furthermore assumed that the effect of the upstream history in the boundary layer as Maffulli (2013) describes, may also be important. Moreover, the upper half of the rib front is exposed to the reestablishing flow (Fig. 4) and is therefore particularly sensitive to changes in the operating or boundary conditions. This is where the largest differences between the two simulations appear as well as as where differences between both simulations and the experiment occur.

For the practical case of a real turbine blade, assuming a coolant temperature of 900K and a metal temperature at the material limit of 1200K (e.g., Cukurel and Arts, 2013) and a Biot number of order unity, we obtain a temperature difference in the blade of around 10K. Locally, this value may be larger due to larger local enhancement factor differences. Since the life of a turbine blade is reported to be half for an increased temperature of 30K, this temperature difference demonstrates the severe impact of the applied boundary condition on the design application.

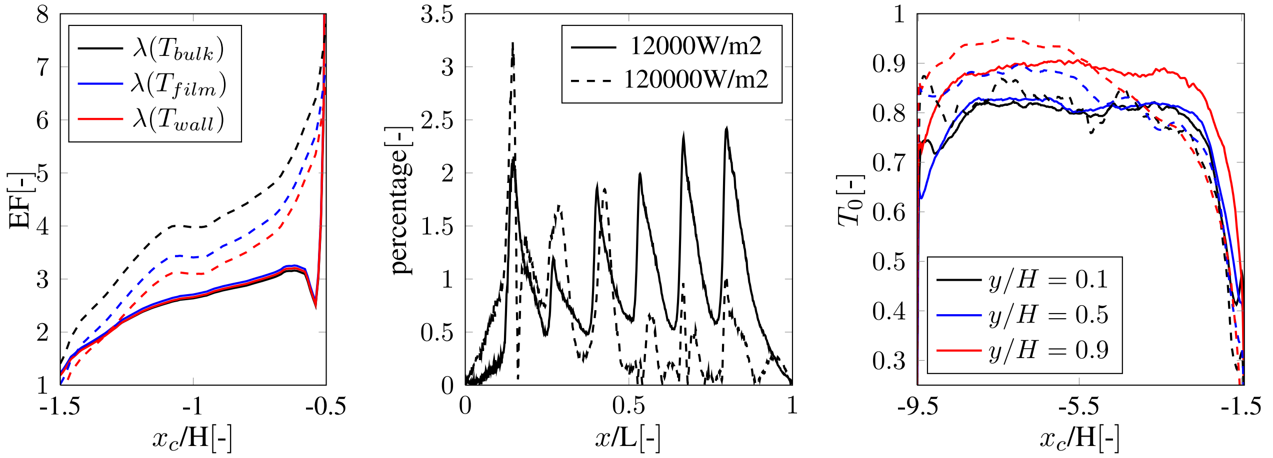

(a) EF at the rib front for different reference temperatures for the fluid conductivity $\lambda(T)$, with $T_{film} = \frac{T_{wall}+T_{bulk}}{2}$.

(b) Used bulk temperature (T_{bulk}) deviation from the centerline temperature ($100 \cdot \frac{T_{center}-T_{bulk}}{T_{bulk}}$) through the whole channel.

(c) Non-dimensionalized temperatures with $T_0 = \frac{T_{wall}-T(x)}{T_{wall}-T_{bulk}}$, perpendicular to rib front at different heights for both cases.

Figure 9: Impacts on the heat transfer coefficient and the EF.

CONCLUSIONS

This contribution shows a non-negligible influence of the thermal boundary condition on the heat transfer coefficient for a turbulent flow of a rib-roughened internal cooling channel, which was investigated using an LES code (AVBP) developed at CERFACS. The results were compared with PIV measurements and with heat transfer and temperature measurements finding a good agreement between the simulations and the experiments. The mean flow structures are well represented in the simulations. The enhancement factor along the channel for the similar scaled computation is also in good agreement with experimental studies. The second simulation with increased flux shows a global difference of 13 % and differs locally by more than 100 %. This means that for temperature predictions with design application the imposition of a constant heat transfer coefficient may lead to significant differences in comparison with the true physics. The cooling channel heat transfer computation can no longer be considered as being decoupled from a solid part and coupled simulations are needed.

ACKNOWLEDGMENTS

The research leading to these results has received funding from the European Community's Seventh Framework Programme (FP7, 2007-2013), PEOPLE programme, under the grant agreement No FP7-290042(COPAGT project).

REFERENCES

T. Arts, C. Benocci, P. Rambaud, *Experimental and Numerical Investigation of Flow and Heat Transfer in a ribbed duct*, 3rd International Symposium on Integrating CFD and Experiments in Aerodynamics, U.S. Air Force Academy, CO, USA, 20-21 June 2007

M. Çakan, *Aero-thermal Investigation of Fixed Rib-roughened Internal Cooling Passages*, Ph.D. Thesis, Universite Catholique de Louvain (UCL) and Von Karman Institute for Fluid Dynamics, ISBN 2-900243-2-X, July 2000.

L. Casarsa, *Aerodynamic performance investigation of a fixed rib-roughened internal cooling passage*, Ph.D. thesis, Universita Degli Studi Udine, Von Karman Instititue for Fluid Dynamics 2003.

L. Casarsa and T. Arts, *Experimental investigation of the aerothermal performance of a high blockage rib-roughened cooling channel*, ASME Journal of Turbomachinery 127, 580-588, 2005.

O. Colin and M. Rudgyard, *Development of high-order taylor-galerkin schemes for unsteady calculations*. Journal of Computational Physics. 162(2), pp338-371, 2000.

O. Colin, A. Benkenida, and C. Angelberger. 3D modeling of mixing, ignition and combustion phenomena in highly stratified gasoline engine. Oil and Gas Science Tech. 58, 1 , 47-62, 111, 2003

Collado E., Gourdain N., Duchaine F., and Gicquel L.Y.M. *Effects of free-stream turbulence on high pressure turbine blade heat transfer predicted by structured and unstructured LES*. Journal of Heat and Mass Transfer, 55(21-22):5754- 5768, 2012.

B. Cukurel, *Conjugate heat transfer investigation of a fixed rib roughened cooling passage*, Ph.D. thesis, Purdue University and Von Karman Institute for Fluid Dynamics, 2012.

B. Cukurel and T. Arts, *Local heat transfer dependency on thermal boundary condition in ribbed cooling channel geometries*, ASME Journal of Heat Transfer 135, 101001-1-101001-11, 2013.

P.W. Dittus, M.K. Boelter, *Heat Transfer in Automobile Radiators of the Tubular Type*, University of California Pub. Eng., Vol. 2, number 13, October, 1930, pp.443-461, reprinted in Int. Comm. Heat Transfer, Vol. 12, pp. 3-22, 1985.

J. Donea and A. Huerta, Finite Element Methods for Flow Problems, John Wiley and Sons, Ltd, Chichester, UK, 2003

F. Duchaine, A. Corpron , V. Moureau , F. Nicoud , T. Poinsot. Development and assessment of a coupled strategy for conjugate heat transfer with Large Eddy Simulation. Application to a cooled turbine blade. International Journal of Heat and Fluid Flow, 30(6): 1129-1141, 2009

A. Fitt, C. Forth, B. Robertson and T. Jones, *Temperature ratio effects in compressible turbulent boundary layers*, International Journal of Heat and Mass Transfer, 29(1), pp. 159-164, Elsevier, 1986.

R. Fransen, N. Gourdain, L.Y.M. Gicquel, *Steady and Unsteady Modeling for Heat Transfer Predictions of High Pressure Turbine Blade Internal Cooling*, Proceedings of ASME Turbo Expo 2012, June 11-15, 2012.

R. Fransen *Simulation aux Grandes Echelles pour la modélisation aérothermique des aubages de turbines refroidies* - TH/CFD/13/35. PhD thesis, Université de Toulouse - MeGeP - Dynamique des Fluides, 2013.

J. Han, S. Dutta, S. Ekkad, *Heat Transfer Cooling Technology*, Taylor and Francis, 2000.

L. He, M. Oldfield, *Unsteady conjugate heat transfer modeling*, ASME Journal of Turbomachinery 133 031022-1-12, 2011.

J. Hunt, A. Wray, P.Moin, *Eddies, streams, and convergence zones in turbulent flows*, Proceedings of the Summer Programm. Center for Turbulence Research, 1988.

C. J. Keylock , T. E. Tokyay and G. Constantinescu *A method for characterizing the sensitivity of turbulent flow fields to the structure of inlet turbulence.* Journal of Turbulence, 12, N45, 2012.

R. Maffulli, L. He, *Wall temperature effects on heat transfer coefficient*, Proceedings of ASME Expo GT2013, 2013.

S. Mendez and F. Nicoud, *Large eddy simulation of a bi-periodic turbulent flow with effusion*. Journal of Fluid Mechanics, 598, pp 27-65., 2008.

F. Nicoud, F. Ducros, *Subgrid-scale stress modelling based on the square of the velocity gradient*. Flow Turb. Combust. 62, 183-200, 1999.

T. Poinsot, and S. Lele,*Boundary Conditions for Direct Simulations of Compressible Viscous Flows*, J. Comput. Phys., 101(1), pp. 104-129, 1992.

P. Sagaut, *Large Eddy Simulations for incompressible flows.* Scientific computation series. Springer-Verlag, 2000.

J. Smagorinsky, *General Circulation Experiments With the Primitive Equations: 1. The Basic Experiment.,* Mon. Weather Rev., 91, pp. 99-164, 1963.

T. Schönfeld and T. Poinsot, *Influence of boundary conditions in LES of premixed combustion instabilities.* Annual Research Briefs. Center for Turbulence Research, NASA Ames and Stanford University, pp. 73-84, 1999.